Journal of Japan Association for Earthquake Engineering, Vol. 25, No. 8, 2025

DEEP SUBSURFACE S-WAVE VELOCITY STRUCTURE IN THE AMAMI ISLANDS, TOKARA ISLANDS, AND YAKUSHIMA ISLAND, JAPAN

Nobuyuki YAMADA[1] and Hiroshi TAKENAKA[2]

[1] Member, Dr. Eng., Professor, Kochi University,
Kochi, Japan, nyamada@kochi-u.ac.jp
[2] Member, Dr. Sc., Professor, Okayama University,
Okayama, Japan, htakenaka@cc.okayama-u.ac.jp

ABSTRACT: In this study, the deep subsurface S-wave velocity (Vs) structure was estimated using microtremor array data on the Amami and Tokara Islands, and Yakushima Island in Japan. The depth of the top of the seismic basement was about 2.0 km, with the largest depth located at Kikaishima Island in the Amami Island Group; the depths at the other islands ranged from 0.2 to 0.6 km. The mean Vs values for each layer and the layer boundary depths at each location under a four-layer model were 0.69, 1.02, 2.18, and 3.49 km/s. These mean values were close to those of the Yaeyama, Miyako, and Okinawa Islands. These results can be used to improve the structural Vs model of the Nansei Islands.

Keywords: *Amami Islands (Yoronjima Island, Okino-Erabujima Island, Tokunoshima Island, Amami-Oshima Island, Kikaishima Island), Tokara Islands (Takarajima Island, Nakanoshima Island), Yakushima Island, Microtremor array exploration, S-wave velocity structure*

1. INTRODUCTION

The Amami Islands, located in the northern part of the Nansei Islands, comprises the islands of Oshima (the largest, hereafter referred to as “Amami-Oshima”), Kikaishima, Tokunoshima, Okino-Erabujima, and Yoronjima and their surrounding islands, as well as the Tokara Islands, which consists of ten inhabited islands, including Nakanoshima and Takarajima. Most of these islands are small and have small populations and social scales. They require vigilance not only against atmospheric and oceanic disasters, such as typhoons and tsunamis, but also against strong ground motion disasters, especially as large earthquakes frequently occur in the surrounding seas. For example, the 1911 Kikaishima earthquake (M 8.0) (Usami[1)]) and the recent 1995 Amami-Oshima earthquake (M_{JMA} 6.7) (e.g., Tsunoda et al.[2)]) have caused considerable damage to Kikaishima Island and the surrounding areas of Amami-Oshima. For the latter earthquake, analysis of strong ground motions from the 1995 earthquake have been attempted (e.g., Takenaka et al.[3)]). In the Tokara Islands, frequent seismic swarms have occurred in the waters surrounding the southern part of the islands, particularly from Takara to Akuseki. This includes an earthquake in December 2021 (Japan Meteorological Agency[4)]) with an intensity of 5 on the Japanese scale. Furthermore, owing to active volcanic activity on the islands of Nakanoshima and

Suwanosejima in the northern part of the Tokara Islands, eruption warnings are frequently issued (Japan Meteorological Agency[5]). Considering such past seismic activities, earthquakes in the Nansei Islands Trench by the Pacific Ocean or near the Okinawa Trough by the East China Sea may cause strong and damaging ground motion (Earthquake Research Promotion Headquarters[6]), heightening concerns regarding future earthquake damage in the various islands. In the event of an earthquake with strong ground motion, in addition to human and property damage, damage to harbors may also occur, which is a significant problem to isolated islands because of their heavy dependence on shipping routes.

Owing to the concern regarding the potentially damaging effects of earthquakes in the Nansei Islands Trench and the Okinawa Trough, the accuracy of ground motion evaluation must be improved for earthquake disaster prevention on the islands. As an important parameter in seismic evaluation, the measurement of S-wave velocity (Vs) structures is necessary to improve the accuracy of deep ground modeling up to the top of the seismic basement, which refers to the Vs 3 km/s equivalent layer. A deep subsurface velocity model of the area has been available at the J-SHIS (National Research Institute for Earth Science and Disaster Prevention[7]) since 2014; however, the geophysical survey information that can be used as a basis for the model properties required for earthquake ground motion evaluation remains limited. Gravity maps (Bouguer anomaly) from Geological Map Navi (National Institute of Advanced Industrial Science and Technology[8]) exist over a wide area in the region, but their correspondence to the velocity structure in this area is uncertain. In the surrounding seas, several resource explorations (e.g., Japan Organization for Metals and Energy Security[9]) and structural explorations of the crust and plates at great depths (e.g., Nishizawa et al.[10]) have been conducted, but except for geological surveys, human living areas on islands with permanent seismic stations have not been explored. Yamada et al.[11] attempted to estimate the subsurface structure at Iojima Island (Fig. 1(b)), which is close to the study area, using microtremor observation data; however, no information has been provided for this study area.

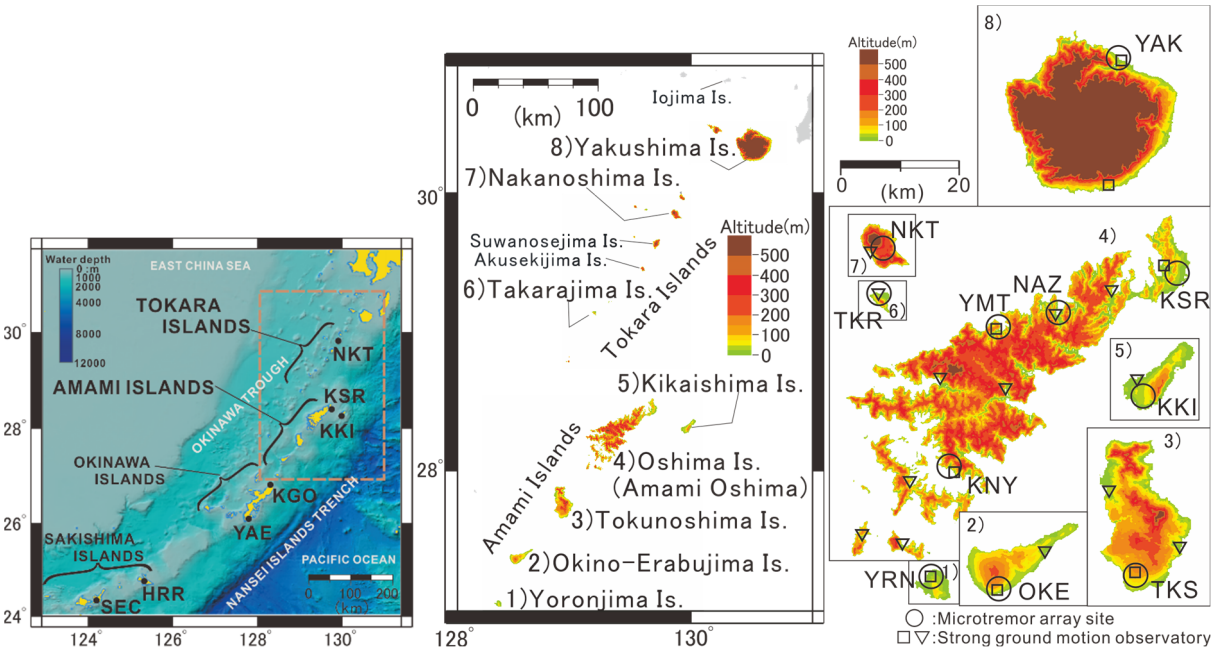

(a) Location of Nansei islands, taken from GSI color-coded elevation map[15] (The black dots correspond to the points shown in Fig. 6.)

(b) Elevation of the Amami and Tokara islands, Yakushima island (The numbers correspond to those in (c).)

(c) Location of exploration and seismic observatories(□ and ▽ show strong-ground motion observatory stations of K-NET and seismic intensity observatory station.)

Fig. 1 Location of main islands, elevation and location of exploration and seismic observatories (The dashed box in (a) indicates the area shown in (b).)

The authors have previously conducted microtremor array observations of long-period ground motion from approximately 0.5 s to several seconds to investigate deep subsurface structures in the Sakishima (Yaeyama and Miyako) Islands and Okinawa Islands in the Nansei Islands the S-wave velocity structures at several locations (Yamada and Takenaka[12), 13)]). This present study aims to describe the results of the deep subsurface Vs structure estimation from the engineering bedrock of about Vs 0.6 km/s to the top of the seismic basement near the strong-motion observation stations on the target islands, and elucidate information for the construction of a numerical model to be used for ground motion prediction and other applications. This study not only explores the deep subsurface structure in the Nansei Islands, but also provides significant data for earthquake disaster prevention. And this study is based on the analysis of the Amami and Tokara Islands in the previous report of Yamada et al.[14)] and additional data from Yakushima Island and a reanalysis of the entire area.

2. TOPOGRAPHY AND GEOLOGY OF TOKARA ISLANDS, AMAMI ISLANDS, AND YAKUSHIMA ISLAND

This study focuses on the islands of Amami (Yoronjima Island, Okino-Erabujima Island, Tokunoshima Island, Amami-Oshima Island, and Kikaishima Island), Tokara (Takarajima Island and Nakanoshima Island), and Yakushima Island (Fig. 1). These islands are scattered over an area of approximately 400 km from north to south, and feature different topographies and geologies. The general geology of each island is shown in Fig. 2(a), which was taken from and added to a simplified version of the seamless geological map (National Institute of Advanced Industrial Science and Technology[16)]). Table 1 describes the geology covering most of the island from GeoMap Navi[8)]. The geological features that cover most of the area of each island were roughly classified into groups (1)–(5) (Table 1) based on their different features. This included (1) coral reef islands such as Yoronjima, Okino-Erabujima, and Kikaishima; (3) an island composed of old accretionary complexes from the formation period of Amami-Oshima; (4) a volcanic island in Nakanoshima; and (2) islands exhibiting mixed geological features such as the islands of Tokunoshima and Takarajima and (5) Yakushima Island. The surface geology near the surveyed sites was sedimentary rock of relatively recent age (light blue area in Fig. 2(a) and rightmost column in Table 1b).

The topography of each island is shown in Fig. 1, with the maximum elevation in Table 1 and the elevation of the exploration sites in Table 2 based on the topographic map[15)]. The islands in group (1) feature relatively flat hills, with many lowlands below an elevation of 50 m (green area in Fig. 1(c)). The islands in the other groups have small areas below 50 m, and are mainly high-elevation areas above 300 m (red and brown areas in Fig. 1(c), especially the islands in (4) and (5), where the elevation exceeds 500 m. The high-elevation topography extends near the coast and is generally steep. The coastline of island (3) has a complex shape. Most of the survey sites were located at elevations of 50 m or less along the coast, except for the sites of this exploration in the Tokunoshima and Nakanoshima Islands, which are located at high elevations. According to the seafloor bathymetry shown in Fig. 1(a), the deep sea caused by the Nansei Islands Trench to the east along the northeast–southwest island chain and the Okinawa Trough to the west are major features.

A gravity diagram [Bouguer anomaly][8)] with an assumed density of 2.67 g/cm^3 is shown in Fig. 2(b). A valley-like region with decreasing values is distributed in a northeast–southwest direction on the east side of the section connecting the Amami-Oshima and Yakushima Island and extends southward to the northeast offshore of the Sakishima Islands. The contours around the Amami Islands were denser in the northwest–southeast direction than in the northeast–southwest direction, with a larger slope of the change. In the Amami Islands and western part of the Tokara Islands, there is an irregularity in the values. On the islands of Tokunoshima, Amami-Oshima, Tokara, and Yakushima, values of approximately 50–60 mgal (gal = cm/s^2) were described, and values of approximately 100 mgal were done on the islands of Yoronjima and Okino-Erabujima. In contrast, Kikaishima Island was characterized by –10 mgal value located in a valley of smaller values compared with those of the other islands.

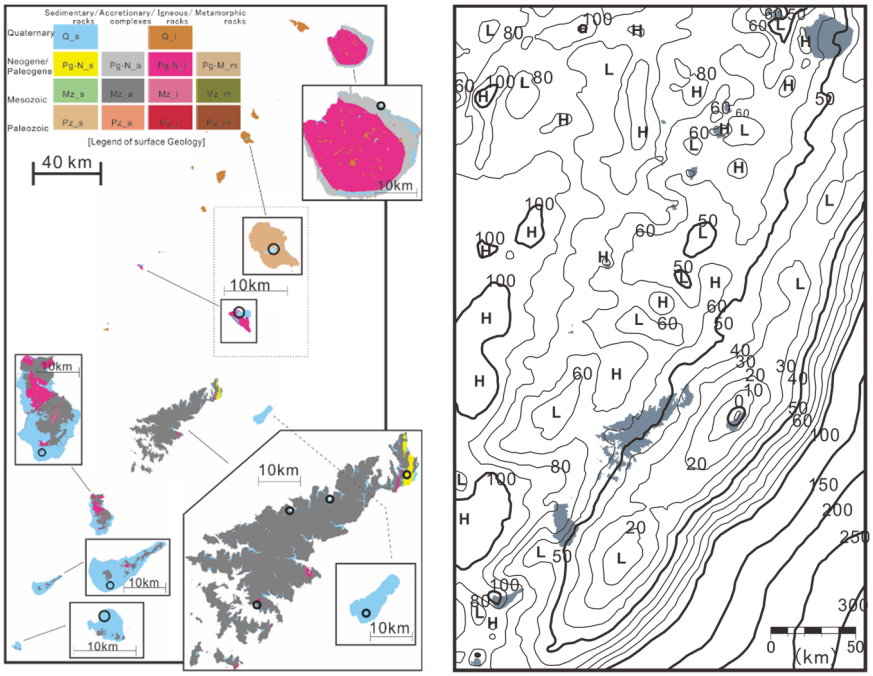

(a) Surface geology of target islands (Circles show exploration sites.)

(b) Gravity map (Bouguer anomaly) contours (in mgal)

Fig. 2 Surface geology and Bouguer anomaly in Amami and Tokara Islands, and Yakushima Island

Table 1a List of the maximum elevations and primary surface geology of the islands

island name	Maximum elevation(m)	Classification	Surface geology covering much of the island		
			Large Classification	Facies	Geologic age
Yoronjima	97	(1)	Sedimentary rock	Marine sedimentary unit/ Limestone	Quaternary Pleistocene
Okino-Erabujima	240	(1)	Sedimentary rock	Marine sedimentary unit/ Limestone	Quaternary Pleistocene
Tokunoshima	645	(2)	Sedimentary rock	Marine sedimentary unit/ Limestone	Quaternary Pleistocene
			Sedimentary complex	Mixed rock/ Cretaceous complex	Late Cretaceous
			Igneous rock	Granite	Palaeogene
Oshima (Amami-Oshima)	694	(3)	Sedimentary complex	Marine sedimentary unit/ Mudstone	Early Cretaceous
			Sedimentary complex	Sand-Mudstone Alternating interbeds	Early Cretaceous
			Sedimentary complex	Mixed rock	Miidle Jurassic
			Sedimentary complex	Marine sedimentary unit/ Sandstone	Late Cretaceous
			Sedimentary rock	Marine terrace depsoit	Quaternary Holocene
Kikaishima	204	(1)	Sedimentary rock	Marine sedimentary unit/ Limestone	Quaternary Pleistocene
Takarajima	292	(2)	Sedimentary rock	Terrace deposit	Quaternary Chibanian
			Sedimentary rock	Marine terrace depsoit/ Sand dune	Quaternary Holocene
			Igneous rock	Andesite	Miocene
Nakanoshima	979	(4)	Igneous rock	Andesite/ Basaltic andesite	Quaternary Holocene
			Igneous rock	Andesite/ Basaltic andesite	Quaternary Chibanian
Yakushima	1936	(5)	Igneous rock	Granite	Miocene
			Sedimentary complex	Marine sedimentary unit/ Sandstone	Eocene
			Sedimentary complex	Marine sedimentary unit/ Mudstone	Eocene

Table 1b List of surficial geology at the exploration sites

island name	Surface geology at the exploration site			
	No.	Code	Large Classification	Facies
Yoronjima	1	YRN	Sedimentary rock	Marine sedimentary unit/ Limestone
Okino-Erabujima	2	OKE	Sedimentary rock	Marine sedimentary unit/ Limestone
Tokunoshima	3	TKS	Sedimentary rock	Marine sedimentary unit/ Limestone
Oshima	4	KNY	Sedimentary rock	Marine terrace depsoit
(Amami-Oshima)	5	YMT	Sedimentary rock	Marine terrace depsoit
	6	NAZ	Sedimentary rock	Marine terrace depsoit
	7	KSR	Sedimentary rock	Marine sedimentary unit/Sand-Mudstone Alternating interbeds
				Conglomerate/ Mudstone
Kikaishima	8	KKI	Sedimentary rock	Marine sedimentary unit/ Limestone
Takarajima	9	TKR	Sedimentary rock	Marine terrace depsoit/ Sand dune
Nakanoshima	10	NKT	Sedimentary rock	Valley-bottom alluvial plain deposit/ Basin fill
Yakushima	11	YAK	Sedimentary rock	Marine sedimentary unit
			Sedimentary rock	Marine terrace depsoit
			Igneous rock	Dacite/ Rhyolite

3. MICROTREMOR ARRAY OBSERVATION

Array microtremor observations were conducted to investigate the Vs structure in the deep subsurface at the target site. Surveys were conducted at 11 sites in the islands of Yoronjima (hereafter YRN), Okino-Erabujima (hereafter OKE), Tokunoshima (hereafter TKS), Amami-Oshima (KNY, YMT, NAZ, KSR), Kikaishima (hereafter KKI), Takarajima (hereafter TKR), Nakanoshima (hereafter NKT), and Yakushima (hereafter YAK), as shown in Figs. 1 and 2 and Table 2. The description of the microtremor array observation and estimation method for the velocity structure are the same as those in a previous report[13]. Figure 3 shows an example of the equipment layout on a coral reef island (YRN), a coral reef island with a low value on the gravity diagram (KKI), and a small basin (NKT) sandwiched between volcanoes on a volcanic island. Seven instruments were placed near the apex of the triangle, with their center of gravity (the origin position, hereafter referred to as the center of the array) and the midpoint of each side recording the microtremors simultaneously during one observation. The position near the center of gravity did not change; however, the arrangement of the remaining six instruments was changed and observed multiple times. The array configuration depends on the conditions at the field survey site. Information on the array observations are shown in Table 2; the location information corresponds to the position near the center of gravity. During the observation, the time length was set to 30–60 min, and the instrument spacing was set in the range of several tens of meters to 2500 m, depending on the conditions at each site. The equipment used for the seven simultaneous observations included an over-damped moving coil accelerometer (SMAR-6A3P: 0.3 to 50.0 Hz flat) manufactured by Akashi Corporation, and data loggers by Hakusan Corporation (* in Table 2), with a built-in amplifier (300 ×) for recorder 1 and an external amplifier (500 ×) for recorders 2 and 3. The seismometers used at YRN and OKE were sensors with only the vertical component, whereas three-component sensors were used at the other sites. All observations were made with 100 Hz sampling, and the internal clocks of the loggers were calibrated with GPS signals to ensure that the time difference between instruments was less than 0.01 s. Positional information was acquired using a handheld GPS, and the error margin was maintained within a few meters.

As shown in Fig. 1(c), the 11 survey points were located near the K-NET strong-ground motion seismic stations (National Research Institute for Earth Science and Disaster Prevention[17]) and the Kagoshima Prefecture municipal seismic intensity meter stations (Yamada et al.[18]). The distance between the center of the array and the strong-motion seismic stations was within a few hundred meters for most points, except those for KKI, KSR, and NKT, and were located into the triangular array of the instrument arrangement.

Vertical acceleration records obtained from the microtremor observations at each location were numerically integrated and converted into velocity records for analysis. Examples of velocity Fourier spectra at YRN, KKI, and NKT are shown in Fig. 4. Although the distances between YRN, KKI, and NKT are approximately 200 km and the record timing of the microtremors varied, they all reported peaks around 2.0–4.0 s. The period of 0.5 s or less is a band where variations are likely to occur due to the artificial environment around the array; however, in the present study, the variations were relatively small. Although the equipment used at the three sites differed, the effects of these differences were minimal. At all sites, well-coherent spectral records were obtained over a bandwidth of a few seconds longer than a 0.3 s period. Therefore, the spectral characteristics between the installation points in the same array observation showed no significant differences. Based on the waveform and Fourier spectrum amplitudes, the aforementioned microtremor data obtained by amplifier magnification were deemed to be sufficiently useful for subsequent analysis. Similar results were obtained for the other exploration sites, with some differences. Figure 3 shows topographic and geological maps[8] overlaid onto the aforementioned observation equipment. The legend symbols for the surface geology are listed in Table 3. The geologies of the target areas were similar (sedimentary rock), but the lithology differed in some areas owing to differences in formation factors, such as fluvial and marine formations. The difference in elevation between the points where the equipment was placed was less than approximately 50 m in the case of the large arrays (L and LL) and within a few meters in the case of the small arrays (S). Therefore, the effect on the results of the deep ground analysis in this report was regarded minimal for all points.

Table 2 Information on the microtremor array observation sites

No.	Island name	City name	Place name	Code	Lon. (°)	Lat. (°)	Height (m)	Date	Time	Array Spacing (m) Max.	Array Spacing (m) Min.	*
1	Yoronjima	Yoron	Chabana	YRN	128.4250	27.0522	50.0	2009/3/2	17:00–24:30	2748	78	1
2	Okino-Erabujima	Chinam	China	OKE	128.5770	27.3359	31.0	2009/3/3	21:30–23:30	757	48	1
3	Tokunoshima	Isen	Isen	TKS	128.9432	27.6835	103.0	2010/2/22 2011/9/1	20:00–20:30 11:15–14:00	1811	84	2
4	Amami-Oshima	Setouchi	Koniya	KNY	129.3123	28.1478	2.4	2011/8/30	17:15–19:00	974	31	2
5	Amami-Oshima	Yamato	Yamato	YMT	129.3962	28.3584	7.0	2010/2/21	21:30–23:00	602	78	2
6	Amami-Oshima	Amami	Naze	NAZ	129.4980	28.3801	1.6	2011/6/22	16:00–18:00	450	30	2
7	Amami-Oshima	Amami	Kasari	KSR	129.7007	28.4393	39.0	2011/8/31	10:40–13:45	1343	103	2
8	Kikashima	Kikai	Kikai	KKI	129.9500	28.2923	49.0	2011/9/2	15:30–20:00	2864	55	2
9	Takarajima	Toshima	Takarajima	TKR	129.2051	29.1530	31.0	2013/10/12	15:00–18:10	1235	56	3
10	Nakanoshima	Toshima	Takao	NKT	129.8744	29.8432	225.0	2013/3/16	11:10–13:10	931	71	3
11	Yakushima	Yakushima	Miyanoura	YAK	130.5720	30.4245	2.2	2012/3/14	14:50–17:15	1425	45	3

*:Recorder: 1 = LS8000-SH (16 bit), 2 = LS8000-WD (24 bit), 3 = LS8800 (24 bit)

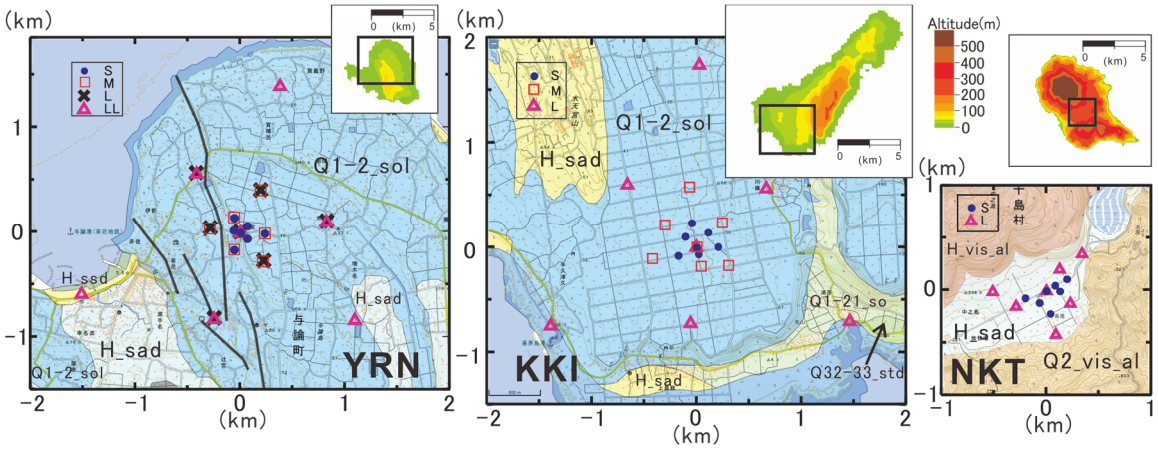

Fig. 3 Examples of the equipment arrangements at sites YRN, KKI and NKT for microtremor array observation. The topographic map and detailed surface geology are overlaid onto a map from Geologic Map Navi. The 'S', 'M', and 'L' indicate the array placement names for observation (Table 3 shows the legend for the surface geology.)

Table 3 Legend symbols for the surface geology in Fig. 3

Legend	Geologic age	Large Classification	Facies
H_sad	Holocene	Sedimentary rock	Marine terrace depsoit
H_ssd	Holocene	Sedimentary rock	Marine terrace depsoit/ Sand dune
Q1-2_sol	Pleistocene	Sedimentary rock	Marine sedimentary unit/ Limestone
Q1-21_so	Pleistocene	Sedimentary rock	Marine sedimentary unit
Q32-33_std	Late Pleistocene	Sedimentary rock	Terrace deposit
H_vis_al	Holocene	Igneous rock	Andesite/Basaltic andesite/Lava/Pyroclastic rock
Q2_vis_al	Pleistocene	Igneous rock	Andesite/Basaltic andesite/Lava/Pyroclastic rock

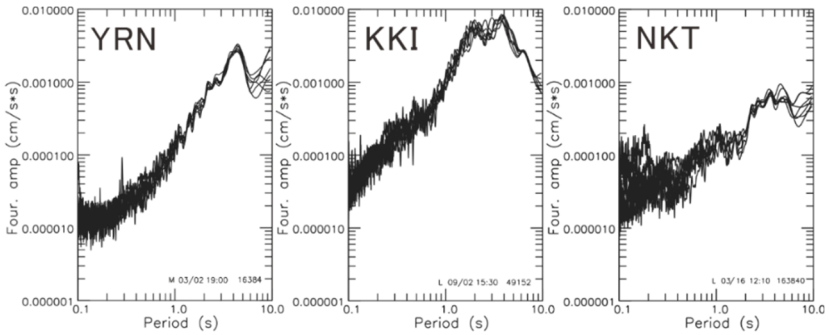

Fig. 4 Example of the velocity Fourier spectrum

4. ESTIMATION OF PHASE VELOCITY

The microtremor records obtained from the observations described in Chapter 3 were divided into datasets every 81.92 s for arrays with small instrumental spacing, and every 163.84 s for the other cases. The recorded intervals used in the analysis excluded portions of the records that were considered to have been significantly influenced by human activities. For each dataset, a frequency–wavenumber spectrum analysis (Capon[19]) was used to calculate the phase velocity from the wavenumber vector at the peak position of the wavenumber spectrum at each frequency, and the average value of the phase velocity for each dataset was used as the final value. These operations were performed for each period, and a value was adopted such that the maximum wavelength of the phase velocity was approximately three to five times the maximum value of the installation point spacing (Okada[20]). The velocity values obtained in each array were continuous to some extent. The phase velocities obtained at each location in each region are shown in Fig. 5. They exhibited dispersion as period increased, and because the vertical component of the recorded data, they were considered the phase velocity of the Rayleigh wave. The obtained phase velocities for the three islands in the southern Amami Islands were similar, ranging from 0.5 to 3.0 km/s; however, in the period ranges from 0.4 to 1.7 s, the slope increased in the order of TKS, YRN, and OKE. Four sites on Amami-Oshima Island were characterized by a lower limit of 1.0 km/s for the KNY and KSR velocity values and a slope change in the KSR above 0.9 s. However, the trend of change was generally similar in the band of periods less than 1.0 s. The period range obtained for the YMT and NAZ sites were narrower than those obtained for the other sites. The phase velocities at the two sites on the Tokara Islands were similar, such as bending at a period of 0.8 s. At YAK, the slope was relatively slow below a period of 0.8 s, but it increased at a period of 1.0 s. In contrast, the KKI sites generally had smaller slopes and longer periods in the 0.5–5.0 s band, which were different from those in the other sites. The obtained phase velocity trends reflected the subsurface structures in each region. Although the correspondence between the trends in the geology and the gravity map described in Fig. 2 was not clear, the phase velocity appeared to have been obtained in a relatively broad band in areas with small values in the gravity map, such as KKI. In contrast, the period range did not significantly narrower in regions where the value was large, such as in YRN and OKE.

Figure 6 shows the phase velocities at the sites on other islands and in the Amami and Tokara areas for comparison. SEC and HRR are in Ishigaki and Miyako Islands[12], respectively, and YES and KGO are in the southeastern and northern parts of Okinawa Island[13], respectively. SEC, KGO, and KSR reported velocity values around 2.5 km/s for periods of 1.0 s or less and exhibited similar variation trends. In contrast, phase velocities of up to about 3.0 s for HRR and YES and up to about 5.0 s for KKI were obtained. Notably, KKI obtained a longer period band than the other islands, although the variation trend of YES was almost the same up to a period of approximately 2.0 s. HRR, which had a similar trend to KKI in that it was obtained over a wide bandwidth and is located in a region with small values in the gravity map[12]. Considering the results of previous studies[12), 13)], site KSR, which was new in this report, was expected to be shallow and have a small number of layers, whereas the KKI was expected to be deep into the seismic basement. This trend in the phase velocity change was also characteristic, and may be deemed a feature of the Nansei Islands when compared with a large number of results.

Because the frequency–wavenumber spectrum method was used to calculate the phase velocity, the direction of arrival of the microtremor can also be determined. Examples of arrival directions for YRN, KKI, and NKT are shown in Fig. 7. In the short period band around 0.5 s, all points indicated arrivals from all directions, but in the YRN and NKT cases (periods around 0.7 s and 1.0 s, respectively), the direction of arrival tended to be biased. For KKI, arrival from all directions were generally obtained for all period bands. These differences among the three islands of similar size may be due to waves and other influences; however, the cause of these trends remains unclear.

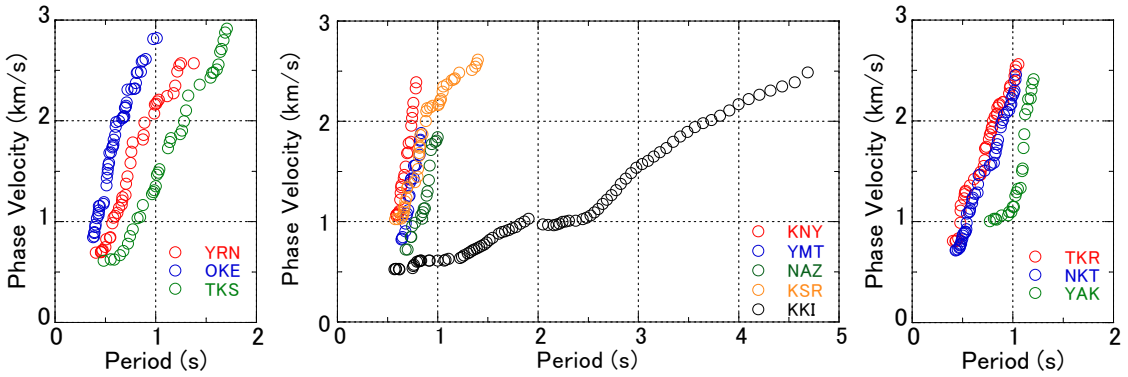

Fig. 5 Phase velocities of the Rayleigh wave at each period obtained from site observation records

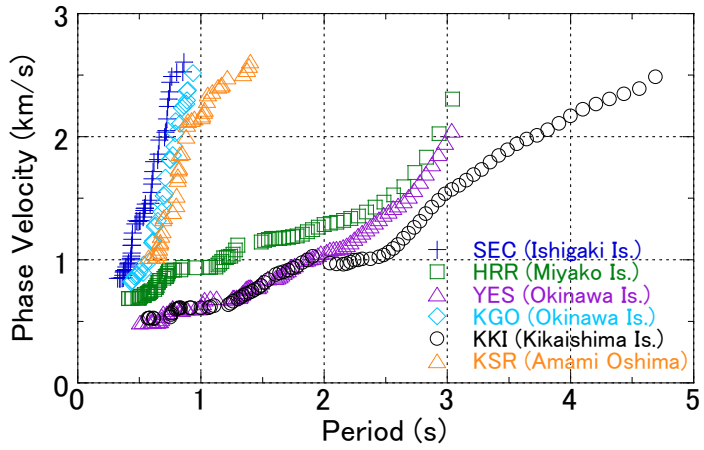

Fig. 6 Comparison of phase velocities at the major sites in the Nansei Islands (Locations correspond to those in Fig. 1(a).)

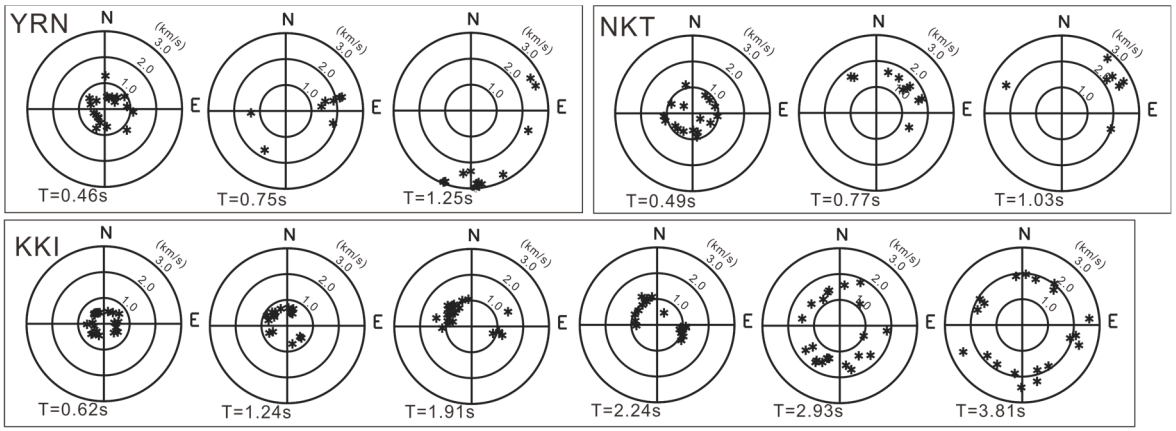

Fig. 7 Examples of the microtremor arrival directions during each period for sites of YRN, KKI, and NKT

5. ESTIMATION OF V_S STRUCTURE

We performed an inverse analysis using a genetic algorithm (Yamanaka and Ishida[21]) to estimate the 1D Vs structure at each site based on the phase velocities obtained from the microtremor observation records (Fig. 5). In the inverse analysis, the fundamental mode of the Rayleigh waves was assumed, and the average of the models fell within the range of the minimum value of the sum of the absolute differences (misfit) between the observed and theoretical values of the phase velocities in each period; consequently, 1.03 times that value was determined to be the optimal model (Yamanaka and Yamada[22]). The procedure for the following inversion was the same as that described in the previous studies[12), 13)]. For the model setting during the inverse analysis, the results from the Okinawa Island, the southern neighbor of the Amami Islands, were used as references. In addition, because the layers with large changes in velocity structures (shown in J-SHIS[7]) were generally layers from 2 to 4 and the phase velocity in Fig. 5, from 2 to 4 layers model (Table 4) was assumed and the search range was set. Because a few information was available regarding the velocity structure in this region, calculations were performed for each of the three cases with 2–4 layers in the inverse analysis. The case with the highest number of solutions within the error tolerance and the best reproducibility of the observed phase velocity was then selected.

Figure 8 shows the estimated Vs structure (0.0 km on surface) called 1st inv.; the gray line (within 3%) represents all models with an error ≤ 1.03 times the minimum misfit from all models obtained in the inverse analysis, and the solid red line (1st inv.) is the mean value. The number of models adopted as acceptable was relatively few at some points (OKE: 16 models); however, more than 25 models were adopted at other points. At YRN, the depth of the basement largely varied, and at YMT and NAZ, there the Vs of the basement showed large variations; hence, the accuracy of the model may be lower than at other sites. However, at most sites, the variation in the Vs and thickness (depth) values of each layer (spread of the gray line) was small. The solutions in the inversion of the depth of the seismic basement in YRN was approximately 0.2 or 1.0 km; however, the number of solutions for the shallower depth was larger, finally, an average value of 0.42 km was obtained for YRN. The Vs values are shown in Fig. 8, and the boundary surface depths of each layer are listed in Table 5. YRN, OKE, TKS, KSR, TKR, and NKT obtained the three-layer model; KNY, YMT, NAZ, and YAK the two-layer model, and only KKI the four-layer model. The overall trend of the Vs values ranged from 0.6 to 1.1 km/s for the first layer near the surface and 3.1 to 3.6 km/s for the deepest layer. This deepest layer corresponds to the seismic basement, although the Vs values were slightly higher at some points. The depths at the top of the seismic basement ranged from 0.2 to 0.4 km at seven sites in the Amami Islands except KKI, was approximately 0.3 km at two sites in the Tokara Islands, and approximately 0.5 km at YAK. The seismic basement depth from the Amami Islands to the Tokara Islands showed little change over a depth range of several hundred meters. In particular, the four sites on Amami-Oshima Island all had seismic basement depths of about 0.3 km and Vs values of approximately 1.0 km/s in the first layer. In contrast, the depth of the seismic basement at KKI was more than 2.0 km, which significantly differed from those at the other sites. The difference in basement depth between the KSR and KKI in the northwest-southeast direction is large. For the part of shallower than the seismic basement, the second layer at the site where the three-layer model was obtained had slightly different Vs values; however, the layer thickness was smaller, such as those in OKE and NKT. Layer 2 thinned out as it moved northward from YRN, OKE, and TKS, disappearing in site KNY in Amami-Oshima Island. For KKI of the Vs values were 0.6, 1.0, and 2.3 km/s. This site featured a large number of layers and a different velocity structure was estimated compared with those in other points.

The theoretical phase velocity of the Rayleigh waves calculated from the Vs structure model shown in Fig. 8 (1st inv.: solid line), and the observed phase velocity (obs.) are shown in Fig. 9. The P-wave velocity used to calculate the theoretical dispersion curve was linked to Vs using an empirical formula (Kitsunezaki et al.[23]). At all sites, the values of the theoretical phase velocity were approximately within the error bars of the observed phase velocity, demonstrating a good correspondence between the two. Therefore, the structural Vs model obtained in this study was able to explain the observed phase velocity. However, the observed phase velocity values obtained at YMT and NAZ were less than 2.0 km/s (period less than 1.0 s), and no higher phase velocity values were obtained. Therefore, the validity of the velocity

structure cannot be adequately determined for parts of the structure above 2.0 km/s, as indicated by the theoretical phase velocity (mainly corresponding to the deeper part of the structure).

Figure 8 also shows the model (gray dashed line) in J-SHIS (version 3.2)[7] overlaid. The Vs values for the near-surface layers were generally close to the present results at all sites. However, the depths at the top of the seismic basement differed and were generally shallower than the present results. For example, the J-SHIS model indicated the top depth of the seismic basement as 2.92 km for KSR and 4.07 km for KKI, whereas the estimated results in this study were 0.41 and 2.06 km, respectively. In addition, the number of layers differed at many sites, with the J-SHIS data showing three to five layers and the thickness of the intermediate layer between the seismic basement and the surface layer was several hundred meters, which differed from the results estimated in this study. Fig. 9 also shows the theoretical phase velocity calculated from the J-SHIS model. Many locations showed large differences with, or did not correspond to, the observed phase velocity.

For KKI, in addition to the four-layer model in Table 4, comparisons are also shown for the three- and five-layer models (Table 6(a)) with the set search range. The observed phase velocities were obtained over a wider bandwidth compared with those at other sites, suggesting a wider range of model selections. The estimation results are listed in Table 6(b), and a comparison of the observed and theoretical phase speeds is shown in Fig. 10. Above a period of 1.0 s, the results for both models overlapped; however, below a period of 1.0 s, the three-layer model case shifted from the observed record. In the case of the four-layer and five-layer models, although there are differences between periods, the differences are small and the reproducibility is almost the same, indicating that a five-layer model may be possible. The five-layer model results in shallower seismic basement depths relative to the four-layer model. However, since we are considering the construction of a numerical model here, we decided to adopt it as a four-layer model, considering the previous results[12), 13)] for the Nansei Islands.

Table 4 Search ranges set for the inverse analysis

Layer	Vs (km/s)	Thickness (km)	Density (g/cm^3)
1	0.4–0.9	0.001–1.0	1.95
2	0.8–1.6	0.001–1.0	2.15
3	1.4–2.5	0.001–2.0	2.35
4	2.3–3.6	∞	2.60

*KKI

Layer	Vs (km/s)	Thickness (km)	Density (g/cm^3)
1	0.4–1.6	0.001–1.0	2.00
2	1.4–2.5	0.001–2.0	2.35
3	2.3–3.6	∞	2.60

*YRN, OKE, TKS, KSR, TKR, NKT

Layer	Vs (km/s)	Thickness (km)	Density (g/cm^3)
1	0.8–2.5	0.001–1.0	2.00
2	2.3–3.6	∞	2.60

*KNY, YMT, NAZ, YAK

(* indicates the location adopted in the 1st inv.)

Table 5 Vs structures (Vs: km/s, D: depth: km) obtained in the 1st inv. for each site

	Range of Vs	YRN		OKE		TKS		KNY		YMT		NAZ		KSR		KKI		TKR		NKT		YAK	
Layer	(km/s)	Vs	D	Vs	D	Vs	D	Vs	D	Vs	D	Vs	D	Vs	D	Vs	D	Vs	D	Vs	D	Vs	D
1	<0.9	0.70	0.21	0.87	0.20	0.63	0.24					0.85	0.37			0.59	0.36	0.59	0.12	0.70	0.19		
2	0.9< <1.6			1.50	0.23			1.08	0.35	0.92	0.33			1.00	0.37	1.02	1.36					1.05	0.53
3	1.6< <2.5	2.00	0.43			2.14	0.25							2.04	0.41	2.30	2.06	1.65	0.32	2.21	0.25		
4	3.0<	3.53	–	3.59	–	3.53	–	3.46	–	3.16	–	3.40	–	3.56	–	3.52	–	3.59	–	3.57	–	3.48	–

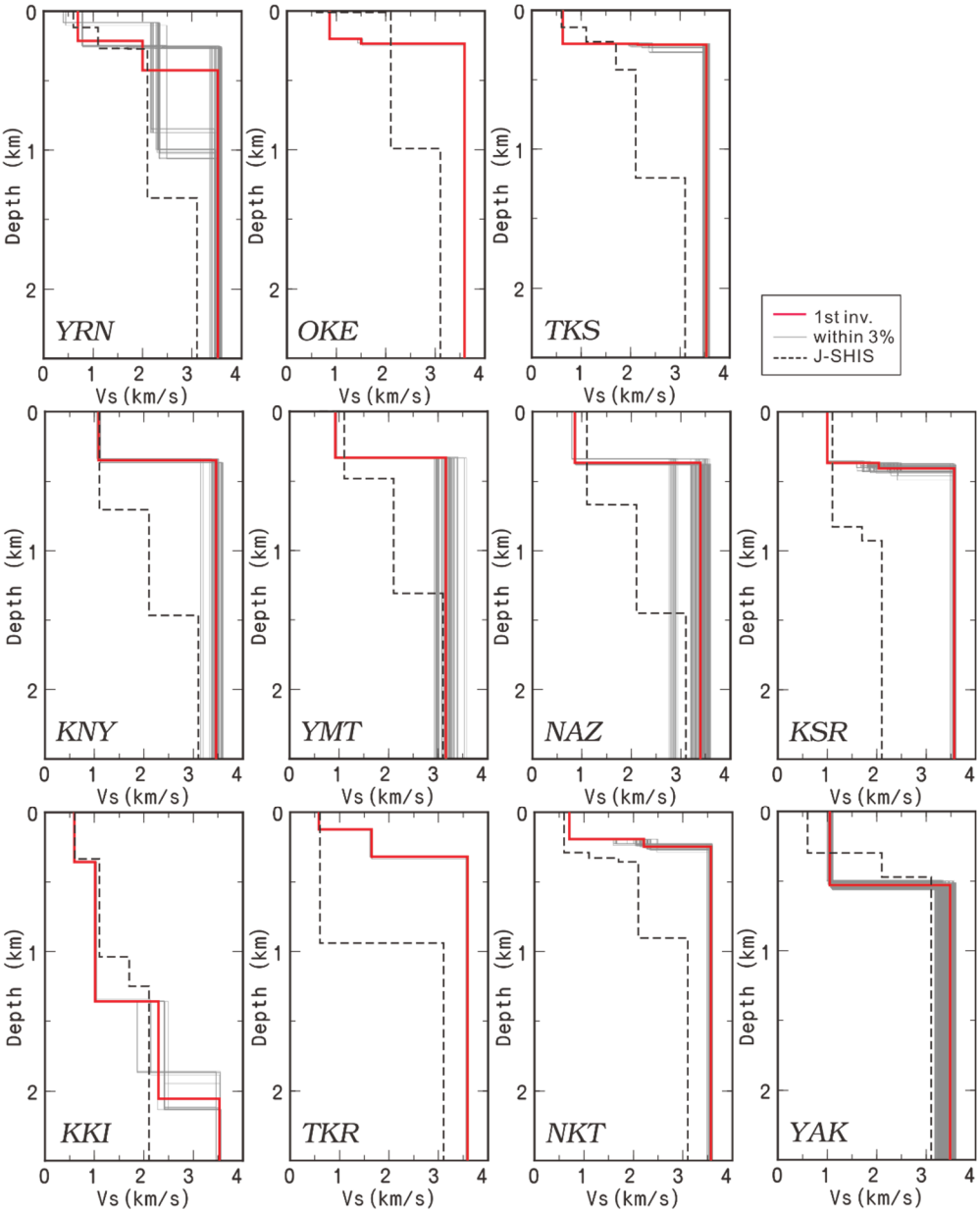

Fig. 8 S-wave velocity structure models for each site (Gray line: within 1.03 times the minimum misfit; red line: averaged model; dashed line: J-SHIS model.)

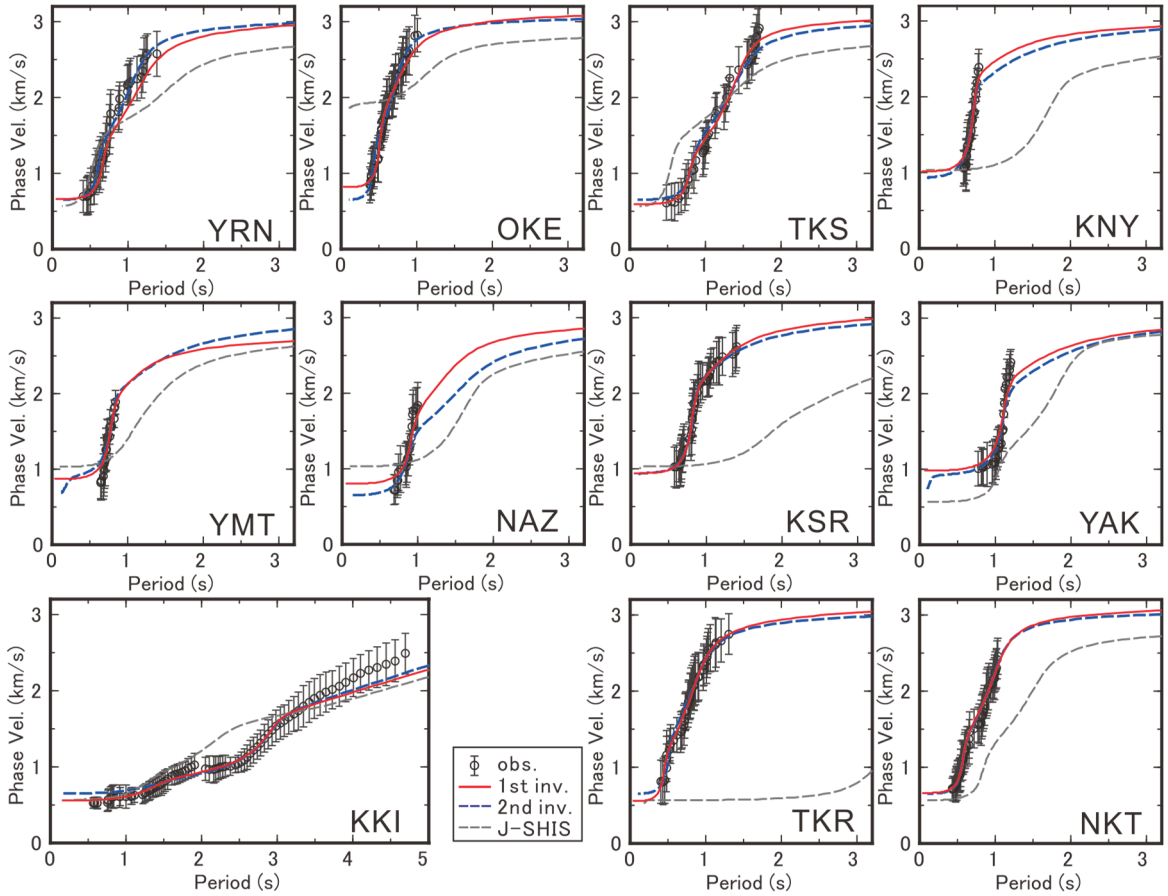

Fig. 9 Comparison of the phase velocities for each site

Table 6 Parameters and results for inverse analysis in KKI

(a) Search range for the five-layer model of KKI

Layer	Vs (km/s)	Thickness (km)	Density (g/cm^3)
1	0.4–0.9	0.001–1.0	1.95
2	0.8–1.6	0.001–1.0	2.15
3	1.2–2.2	0.001–2.0	2.35
4	1.6–2.6	0.001–2.0	2.45
5	2.3–3.6	∞	2.60

(b) V_S structure when assuming the three- and five-layer models

	KKI	3lay
Layer	Vs (km/s)	Depth (km)
1	0.73	0.74
2	1.41	2.06
3	3.53	–

	KKI	5lay
Layer	Vs (km/s)	Depth (km)
1	0.58	0.36
2	1.05	1.35
3	1.78	1.82
4	2.18	1.92
5	3.56	–

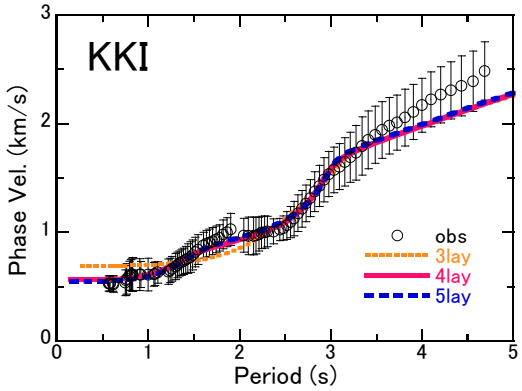

Fig. 10 Comparison of the phase velocities in KKI under the three- (3lay), four- (4lay), and five-layer (5lay) models

6. AVERAGED V_S AND BOUNDARY DEPTH OF EACH LAYER FOR NUMERICAL MODELING

The numerical models of the subsurface structures using the finite difference method, which is used in ground motion simulations, often include homogeneous values of the medium properties within each layer. Therefore, based on the results of the previous chapter, we presented the averaged Vs value and the boundary depths of each layer as model information to facilitate the creation of a 3D numerical model of the subsurface structure, in which the entire domain is treated as having the same number of layers and homogeneity within the layers. Although a structural model with fewer layers was estimated in the 1st inv., we treated it as four layers, similar to the procedures for the Sakishima and Okinawa Islands[12), 13)]. For the 1st to 3rd layer from geo-surface, a weighted average was obtained using the layer thickness values as weights, and for the fourth layer, an additive average of the Vs values was obtained. The Vs values of < 0.9, 0.9–1.6, 1.6–2.5, and ≥ 3.0 km/s were treated as layers 1, 2, 3, and 4, respectively, as shown in Table 5. Note that the layer classification in Table 5 is based on the upper limit of the search range of the four-layer model in Table 4, and the layers are classified according to the Vs values. However, some sites, such as OKE and YMT, reported Vs values that were close to the limit of the search range, necessitating further study on this classification. These results yielded the average Vs values listed in Table 7. Although the survey sites were somewhat far from each other, the average S-wave velocities for the Amami and Tokara Islands, and Yakushima Island were still obtained. The average VS values in the other regions are also listed in Table 7. Although slightly different, the mean Vs values for the islands of Sakishima, Okinawa, Amami, and Tokara were close to each other. Therefore, even if each island in the Nansei Islands is far apart, the numerical model of the velocity structure can be set up with common parameters such as Vs values.

Using the average Vs values obtained, the layer thickness values at each site were again estimated from the inverse analysis, assuming the four-layer model. This result was called the 2nd inv. The procedure for the inversion was the same as that described above, with the Vs values fixed at the averaged values in Table 7 for the search ranges shown in Table 8, and the values in Table 4 (set for the four-layer model) for the other parameters used as is. The layer boundary depths obtained in this study are listed in Table 9. The theoretical phase velocities of the Rayleigh waves of the fundamental mode estimated from the obtained velocity structure model are indicated by the blue dashed line (2nd inv.) in Fig. 9. In the comparison of the phase velocities (Fig. 9), the results for fixed Vs values differed in NAZ; however, at many other locations, the values were close to those obtained by the initial estimation model (1st inv.: red dotted line) and corresponded well with the observed phase velocities (obs.).

Figure 11 shows the results for the Amami Islands for the 2nd inv. (Table 9). As the Vs values for each layer were the same at all sites, the depths of the layer boundaries were compared. According to the results, the depths of the boundaries of layers 1–4 in the southern Amami Islands (YRN, OKE, and TKS) were similar in shape, ranging from 0.2 to 0.3 km. Four sites on Amami-Oshima Island were slightly deeper than those at the three sites on the southern Amami Islands. However, for NAZ, the depth of the boundary between layers 3 and 4 was significantly greater. In the comparison of the phase velocity of NAZ in Fig. 9, the difference between the values of the phase velocity by the 2nd inv. and the observed value is large around the period 1.0 s, and outside the error bar, as mentioned above. This may be because the two-layer models of layers 1 and 4 obtained in the 1st inv. were fixed in the 2nd inv. under the four-layer model, which caused a detrimental effect.

Table 7 Averaged Vs for Sakishima Islands, Okinawa Islands and this study (Amami and Tokara Islands, and Yakushima Island)

	Sakishima Islands[12)]	Okinawa Islands[13)]	This study
Layer	Vs (km/s)	Vs (km/s)	Vs (km/s)
1	0.69	0.69	0.69
2	1.08	1.10	1.02
3	1.74	2.01	2.18
4	3.44	3.46	3.49

Table 8 Search range for re-inverse analysis (2nd inv.) with fixed velocity values

Layer	Vs (km/s)	Thickness (km)	Density (g/cm^3)
1	0.69	0.001–1.0	1.95
2	1.02	0.001–1.0	2.15
3	2.18	0.001–2.0	2.35
4	3.49	∞	2.60

Table 9 Depth of layer boundary (in km) of the model (2nd inv.) obtained from the inverse analysis with fixed Vs values

Layer boundary	YRN	OKE	TKS	KNY	YMT	NAZ	KSR	KKI	TKR	NKT	YAK
1–2	0.19	0.13	0.25	0.01	0.06	0.23	0.01	0.45	0.15	0.19	0.04
2–3	0.22	0.15	0.31	0.30	0.35	0.34	0.38	1.40	0.19	0.19	0.51
3–4	0.29	0.17	0.32	0.55	0.62	1.15	0.40	1.54	0.31	0.21	0.58

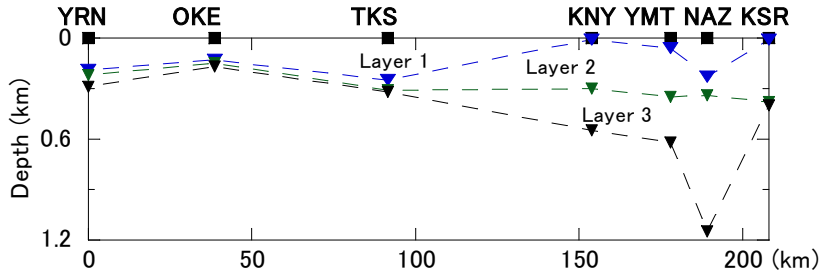

Fig. 11 Depth of the layer boundary in the Amami Islands based on the results of the 2nd inv.

7. CONCLUSION

This study estimated the Vs structure from the geo-surface to the seismic basement using microtremor array observation records at 11 sites near strong-motion stations in the Amami and Tokara Islands, and Yakushima Island. We found that the depth of the seismic basement was approximately 2.0 km at the site in Kikaishima Island, and 0.2–0.6 km at the sites in the other islands. The Vs averages for each layer and the depth of the layer boundary at each site were also shown using a four-layer model that was based on the estimation results for all sites. The average S-wave velocities of the four layers were 0.69, 1.02, 2.18, and 3.49 km/s, which were close to the values of the Sakishima and Okinawa Islands. These results can be used to improve the Vs structural model of the Nansei Islands. In the future, the validity of the obtained velocity structure model should be examined through, for example, 3D ground motion simulation and observed ground motion record analysis to further enhance the structural model. In addition, at the sites where microtremors were recorded by the three-component sensor, the shallow part

of the subsurface could be considered by the H/V spectral ratio (Spectral ratio of horizontal to vertical motion), and the results should be reflected in the modeling.

ACKNOWLEDGMENT

The microtremor array observations in this study were conducted with the cooperation of students from the Faculty of Science and Graduate School of Natural Science and Technology, Okayama University, the Graduate School of Science, Kyushu University, and the Faculty of Education, Fukuoka University of Education. GMT (Wessel and Smith[24]) was used to draw the map. We would also like to thank the three anonymous reviewers and the editorial staff for their very thorough review, which helped us to improve this paper. A part of the results of this research was supported by JSPS Grants-in-Aid for Scientific Research (B) 23310122, 26282105 and 22H01311. We would like to thank everyone involved.

REFERENCES

1) Usami, T.: *Materials for Comprehensive List of Destructive Earthquakes in Japan*, University of Tokyo Press, 493 pp., 1996 (in Japanese).
2) Kakuta, T., Goto, K., Miyamachi, H., Hirano, S., Shimizu, C., Iwakiri, K., Nakatsuji, T. and Tateyama, S.: The 1995 Amami-Oshima-Kinkai Earthquake―Activities and Damage―, *Journal of Geology*, Vol. 106, No. 4, pp. 476–485, 1997 (in Japanese).
3) Takenaka, H., Fujii, Y., Okumura, T. and Suzuki S.: Modeling of Strong Motion at Kikai Island Due to Aftershocks of the 1995 Amami-Oshima-Kinkai Earthquakes, *Journal of Geology*, Vol. 106, No. 4, pp. 525–536, 1997 (in Japanese).
4) Japan Meteorological Agency: Monthly Report on Earthquakes and Volcanoes in Japan December 2021, Seismic Activity in the Seas around the Tokara Islands (near Kodakarajima Island), pp. 24–27, 2021 (in Japanese, title translated by the authors). https://www.data.jma.go.jp/eqev/data/gaikyo/monthly/202112/202112kyusyu_kobetsu_1.pdf (last accessed on February 11, 2025)
5) Japan Meteorological Agency: Volcanic Warnings / Eruption Notice (Toshima Village), 2023 (in Japanese). https://www.jma.go.jp/bosai/map.html#8/29.781/129.773/&contents=volcano (last accessed on February 11, 2025)
6) Headquarters for Earthquake Research Promotion: National Seismic Hazard Maps for Japan (2020), 2021 (in Japanese). https://www.jishin.go.jp/evaluation/seismic_hazard_map/shm_report/shm_report_2020/ (last accessed on February 11, 2025)
7) National Research Institute for Earth Science and Disaster Resilience: Japan Seismic Hazard Information Station. https://www.j-shis.bosai.go.jp/en/ (last accessed on February 11, 2025)
8) National Institute of Advanced Industrial Science and Technology / Geological Survey of Japan, GeomapNavi. https://gbank.gsj.jp/geonavi/?lang=en (last accessed on February 11, 2025)
9) Japan Organization for Metals and Energy Security, New Discovery of Promising Seafloor Hydrothermal Deposit Offshore Amami-Oshima Island, 2020 (in Japanese, title translated by the authors). https://www.jogmec.go.jp/news/release/news_01_000151.html (last accessed on February 11, 2025)
10) Nishizawa, A., Kaneda, K., Oikawa, M., Horiuchi, D., Fujioka, Y. and Okada, C.: Variations in Seismic Velocity Distribution along the Ryukyu (Nansei-Shoto) Trench Subduction Zone at the Northwestern End of the Philippine Sea Plate, *Earth, Planets and Space*, Vol. 69, 86, 2017. https://doi.org/10.1186/s40623-017-0674-7
11) Yamada, M., Ito, Y., Nagao, T., Nozu, A., Nagasaka, Y. and Oiwane H.: Analysis of Site Amplification Factors with the Peak in Low Frequency Band in Satsuma-Iwojima island, *Journal of Japan Society of Civil Engineers*, Ser. A1, Vol. 72, No. 4, pp. 691–699, 2016 (in Japanese).
12) Yamada, N. and Takenaka, H.: Deep Subsurface S-Wave Structure of Sakishima (Miyako and Yaeyama) Islands, Southwestern Japan, *Journal of Japan Association for Earthquake Engineering*,

Vol. 18, No. 1, pp. 77–88, 2018 (in Japanese). https://doi.org/10.5610/jaee.18.1_77
13) Yamada, N. and Takenaka, H.: Deep Subsurface S-Wave Velocity Structure of Okinawa Islands, Japan, *Journal of Japan Association for Earthquake Engineering,* Vol. 21, No. 3, pp. 119–134, 2021. https://doi.org /10.5610/jaee.21.3_119
14) Yamada, N., Takenaka, H. and Komatsu, M.: Deep Subsurface S-Wave Velocity Structure in the Amami and Tokara Islands, Japan, inferred from microtremor array explorations, *The 15th Japan Earthquake Engineering Symposium*, PS1-01-11, 2018.
15) Geospatial Information Authority of Japan, GSI Maps. https://maps.gsi.go.jp/ (last accessed on February 11, 2025)
16) National Institute of Advanced Industrial Science and Technology / Geological Survey of Japan, Seamless Geological Map of Japan at 1:200,000 V2 (in Japanese, title translated by the authors). https://gbank.gsj.jp/seamless/ (last accessed on February 11, 2025)
17) National Research Institute for Earth Science and Disaster Resilience: NIED K-NET, KiK-net, National Research Institute for Earth Science and Disaster Resilience, 2019. https://doi.org/10.17598/nied.0004
18) Yamada, N., Asano, K. and Iwata, T.: Overview of Ground Motions on the Islands of Kagoshima, Japan―Using Seismograph Data of Kagoshima Prefecture―, *The 2020 Seismological Society of Japan Fall Meeting*, S16P-02, 2020.
19) Capon, J.: High-Resolution Frequency-Wavenumber Spectrum Analysis, *Proceedings of the Institute of Electrical and Electronics Engineers*, Vol. 57, pp. 1408–1418, 1969.
20) Okada, H.: Method of Estimation the Subsurface Structure by Microtremor Use, *Geophysical Exploration Handbook*, The Society of Exploration Geophysics of Japan, pp. 203–211, 1998 (in Japanese).
21) Yamanaka, H. and Ishida, H.: Application of Genetic Algorithms to an Inversion of Surface-Wave Dispersion Data, *Bulletin of the Seismological Society of America*, Vol. 86, pp. 436–444, 1996.
22) Yamanaka, H. and Yamada, N.: Estimation of 3D S-Wave Velocity Model of Deep Sedimentary Layers in Kanto Plain, Japan, Using Microtremor Array Measurements, *BUTSURITANSA*, Vol. 55, pp. 56–65, 2002 (in Japanese).
23) Kitsunezaki, C., Goto, N., Kobayashi, Y., Ikawa, T., Horike, M., Saito, T., Kuroda, T., Yamane, K. and Okuzumi, K.: Estimation of P- and S-Wave Velocities in Deep Soil Deposits for Evaluating Ground Vibrations in Earthquake, *Japan Society for Natural Disaster Science*, Vol. 9, No. 2, pp. 1–17, 1990 (in Japanese).
24) Wessel, P. and Smith, W. H. F.: New, Improved Version of the Generic Mapping Tools Released, *Eos, Transactions American Geophysical Union*, Vol. 79, No. 47, p. 579, 1998. https://doi.org/10.1029/98EO00426

(Original Japanese Paper Published: November, 2023)
(English Version Submitted: February 17, 2025)
(English Version Accepted: April 17, 2025)